Manuscript prepared for Solid Earth
with version 2014/09/16 7.15 Copernicus papers of the LaTeX class copernicus.cls.
Date: 11 May 2015

Poroelastic responses of confined aquifers to subsurface strain changes and their use for volcano monitoring

K Strehlow, JH Gottsmann, and AC Rust

School of Earth Sciences, University of Bristol, Wills Memorial Building, Bristol BS8 1RJ, UK

Correspondence to: Karen Strehlow (karen.strehlow@bristol.ac.uk)

Abstract.

Well water level changes associated with magmatic unrest can be interpreted as a result of pore pressure changes in the aquifer due to crustal deformation, and so could provide constraints on the subsurface processes causing this strain. We use Finite Element Analysis to demonstrate the response of aquifers to volumetric strain induced by pressurised magma reservoirs. Two different aquifers are invoked - an unconsolidated pyroclastic deposit and a vesicular lava flow - and embedded in an impermeable crust, overlying a magma chamber. The time-dependent, fully coupled models simulate crustal deformation accompanying chamber pressurisation and the resulting hydraulic head changes as well as porous flow in the aquifer. The simulated deformational strain leads to centimetres (pyroclastic aquifer) to meters (lava flow aquifer) of hydraulic head changes; both strain and hydraulic head change with time due to substantial porous flow in the hydrological system.

Well level changes are particularly sensitive to chamber volume and shape, followed by chamber depth and the phase of the pore fluid. The Young's Modulus and permeability of the aquifer, as well as the strength of pressurisation also have significant influence on the hydraulic head signal. While source characteristics, the distance between chamber and aquifer and the elastic stratigraphy determine the strain field and its partitioning, flow and coupling parameters define how the aquifer responds to this strain and how signals change with time.

We investigated a period of pre-eruptive head changes recorded at Usu volcano, Japan, where well data were interpreted using an analytical deformation model. We find that generic analytical models can fail to capture the complex pre-eruptive subsurface mechanics leading to well level changes, due to aquifer pressure changes being sensitive to chamber shape and lithological heterogeneities. In addition, the presence of a pore fluid and its flow have a significant influence on the strain signal in the aquifer and are commonly neglected in analytical models. These findings highlight the need for numerical models for the interpretation of observed well level signals. However, simulated water table changes do mirror volumetric strain and wells can therefore serve as comparatively cheap strain meters that could provide important insights into pre-eruptive dynamics.

1 Introduction

Pre-, syn- and post-eruptive changes in water levels have been reported for several volcanoes (Newhall et al., 2001). Examples include well water level changes of more than $9\mathrm{m}$ preceding the 2000 eruption of Usu volcano, Japan (Matsumoto et al., 2002) and the water level rise of more than $85\mathrm{m}$ in a geothermal well at Krafla volcano, Iceland, associated with a dyke intrusion in 1977 (Stefansson, 1981). The observed phenomena can often be explained by poroelasticity (Wang, 2000). Compression or dilatation of an elastic porous medium leads to a decrease or an increase in pore space, respectively, which in turn influences the pore pressure and thereby the water level. Hence, one of the proposed interpretations of measured well level changes is a strain-induced change in pore pressure

in the aquifer due to crustal deformation. This is in line with observations of water level changes accompanying seismic events (e.g., Roeloffs, 1996; Jonsson et al., 2003; Shibata et al., 2010) or crustal spreading, as observed at the Juan de Fuca Ridge (Davis et al., 2001).

In volcanic environments, many processes can lead to substantial strain changes, including pressure changes in magma reservoirs and intruding dykes. Information about the local strain field is therefore highly valuable for volcano monitoring and eruption forecasting, as it could allow derivation of these subsurface magmatic processes (e.g., Linde et al., 2010; Bonaccorso et al., 2012; Voight et al., 2006). As strainmeters are complex and expensive installations, the described poroelastic relations raise the question whether we could use wells in aquifers as cheaper and somewhat simpler strainmeters.

Previous studies have indeed utilised the poroelastic behaviour of aquifers to infer magmatic processes from observed water level changes at volcanoes (e.g., Shibata and Akita, 2001; Takahashi et al., 2012). A method of assessing the strain sensitivity of an aquifer is to track water level changes as a result of predictable excitations such as Earth tides or measured barometric variations. The known strain sensitivity is then used to derive volumetric strain from observed water level changes during unrest, and combining this with analytical deformation models such as the Mogi model (Mogi, 1958), inferences can be made on magmatic drivers behind the level changes.

However, oversimplification of the coupling between solid and fluid mechanics may make these models inadequate. An example is the 2000 Usu eruption, where the pre-eruptive water table changes observed in two different wells apparently give inconsistent information about the source of strain. Only one of the two well level changes agrees with the model proposed by Matsumoto et al. (2002). In order to make reasonable monitoring interpretations based on well level data, we therefore need to improve our understanding of how these hydrological signals are generated and identify the relative importance of the parameters that affect the water level changes. Changes in the hydrological conditions in volcanic areas are usually interpreted as a result of changes in the magmatic system, but the effects of non-magmatic parameters on the pressure-response in the aquifer should also be considered.

Numerical modelling of pressure changes in hydrological systems has focused on pressure and temperature transients in hydrothermal systems and resulting ground deformation due to the injection of hot magmatic fluids, using one-way coupling of solid deformation and porous flow (e.g., Chiodini et al., 2012; Fournier and Chardot, 2012). Fracture flow is another suggested mechanism, especially for large water level changes. Numerical investigations have not yet explored whether pure deformational strain can induce equally high head changes. The full, two-way coupling of fluid and solid mechanics required has so far been avoided, and so the effect of solid deformation on pore pressure and porous flow has been neglected.

We investigate the phenomenon of poroelastic responses to magmatic strain changes to better understand the hydrological signals one might observe in wells on a volcano before and during erup-

tions. We assess to what extent confined aquifers can serve as indicators of stress/strain partitioning in the shallow crust due to reservoir pressure changes and therefore if they could provide a tool to scrutinise pre-eruption processes. Our findings help to shed light on the water level changes observed at Usu volcano and provide possible scenarios that explain the discrepancy between the previously suggested model and observations.

2 Methods

Table 1 gives a list of all symbols used in this study.

2.1 Theory

We present a set of generic models using Finite Element Analysis to perform parametric studies on several volcanic settings with an inflating magma chamber affecting overlying rock layers and hydrology. The models solve a series of constitutive equations that result from the full coupling of continuum mechanics equation for stress-strain relations of a linear elastic material with Darcy's law and mass conservation within the porous flow theory (for details see Wang (2000) and COMSOL (2013)). The calculations are based on the Navier equation for a solid:

$$-\nabla \cdot \sigma = \mathbf{F}_V, \tag{1}$$

with σ being the stress tensor and $\mathbf{F}_V$ a body force. Inertia terms in the Navier equation are neglected as the solid deformation is treated as quasi-static. The solid mechanics equations assume linear elasticity and do not allow for material failure, hence only work for sufficiently small strains. The stress tensor σ is related to the strain tensor ϵ and the pore pressure p_f by a generalised Hooke's Law:

$$\sigma - \sigma_0 = \mathbf{C} : (\epsilon - \epsilon_0) - \alpha p_f \mathbf{I}. \tag{2}$$

Here, $\mathbf{C}$ is the drained elasticity tensor and α is the Biot-Willis-coefficient. Strain is given through the displacement vector ($\boldsymbol{u}$) :

$$\epsilon = \frac{1}{2}[(\nabla \boldsymbol{u})^T + \nabla \boldsymbol{u} + (\nabla \boldsymbol{u})^T \nabla \boldsymbol{u}]. \tag{3}$$

Fluid flow is described by mass conservation

$$\rho_f \mathrm{S} \frac{\partial p_f}{\partial t} + \nabla \cdot (\rho_f \boldsymbol{v}) = \mathrm{Q} - \rho_f \alpha \frac{\partial \epsilon_{vol}}{\partial t} \tag{4}$$

and Darcy's law:

$$\boldsymbol{v} = -\frac{\kappa}{\mu}\nabla p_f. \tag{5}$$

Here, ρ_f is the fluid density, S is the storage coefficient, $\boldsymbol{v}$ is fluid flow velocity, Q is a source/sink term, ϵ_{vol} is the volumetric strain, κ is aquifer permeability and μ is water viscosity. The equations for fluid flow only consider single-phase, single-component flow. Gravity effects are neglected; hence we consider an initial hydrostatic state, which is then perturbed by strain changes. Resulting head changes are therefore a pure poroelastic response to the surrounding strain changes. The aquifer is considered to be fully saturated and perfectly confined at all times.

In both Eq. (2) and (4), the terms including the Biot-Willis coefficient describe the coupling between solid deformation and fluid flow, which manifests in stress absorption by the fluid and pore pressure changes due to the increase/decrease of pore space resulting from volumetric changes of the porous medium. The coupling parameter α is a measure of the strength of the coupling (having values between the porosity of the medium and 1), and is defined by the volume of fluid expelled from/sucked into a porous medium when subject to volumetric change.

Finally, the storage coefficient is expressed as:

$$\mathrm{S} = \phi\chi_f + \frac{(\alpha-\phi)(1-\alpha)}{\mathrm{K}}, \tag{6}$$

with ϕ being the porosity of the porous medium, χ_f the fluid compressibility, and K the drained bulk modulus of the solid matrix. This expression for storage also involves further coupling between the solid matrix and the pore fluid.

This set of equations is solved for solid deformation ($\boldsymbol{u}$) and fluid pressure (p_f) using the poroelasticity module of COMSOL Multiphysics, version 5.0. To validate our numerical approach to solve poroelastic problems, we compared a numerically derived solution to the analytical solution for "Terzaghi's compaction", the compaction of a homogeneous poroelastic block. In general, there is a good agreement; the largest errors of about 2% occur only very early in the simulation, close to the pressurised boundary, highlighting the need for mesh refinement close to this boundary (see discussion in Appendix A).

2.2 Model set up

As a starting point to investigate hydrological responses to magma chamber inflation, we build a 2D-axisymmetric model geometry in COMSOL Multiphysics following Hickey and Gottsmann (2014), who provide guidelines for volcano deformation modelling using Finite Element Analysis. The initial model consists of a linear elastic solid block with an embedded spherical cavity, representing a magma chamber at depth. This cavity is pressurised by applying a boundary load. Magma chamber

pressurisation can be generated by the injection of fresh magma, vesiculation, thermal expansion of the magma, melting of country rocks or volume changes during crystallisation (Fagents et al., 2013). Using the relation for temperature independent volume changes

$$\Delta P = \frac{1}{\beta}\frac{\Delta \mathrm{V}}{\mathrm{V}} \tag{7}$$

and assuming a magma compressibility of about $\beta = 10^{-11} Pa^{-1}$, a pressurisation of $10\mathrm{MPa}$ could correspond to a volume change of $\Delta \mathrm{V} = 100,000 m^3$. Note that $\Delta \mathrm{V}$ is not realised in the presented models, as the magma chamber is represented by a pressurised cavity; the value only serves as a guide to corresponding magmatic processes. The resulting deformation of the surrounding material is calculated by discretising the model domain to solve the constitutive equations for continuum mechanics for stress-strain relations of a linear elastic material. Boundary conditions are also taken from Hickey and Gottsmann (2014): the Earth's surface is treated as a free surface, the bottom boundary is fixed and the lateral boundary has a roller condition (free lateral, but no vertical displacement). We then adapt this model setup for our purposes by adding a shallow, rectangular, poroelastic aquifer, which is saturated with water. The internal boundary conditions bordering the aquifer domain are (a) no flow and (b) continuous stress and displacement. To directly model the pressure change relative to any initial pressure condition, the initial pore pressure is set as $0\mathrm{Pa}$. Duration of the time-dependent simulation is 1000 days. We solve the full set of coupled equations, giving solid displacement $\boldsymbol{u}$ and fluid pore pressure p_f. To demonstrate its meaning for water table changes that could be observed during volcanic unrest, we present all results as hydraulic head h, which is proportional to pore pressure:

$$h = \frac{p_f}{\rho_f * g}. \tag{8}$$

It represents the maximum water level change in a small diameter well (ideally a piezometer) in a confined aquifer. The final model set up is shown in Fig. 1; reference values of geometric parameters can be found in Table 2.

The linear elastic material surrounding the magma chamber, from here on called "host rock", has elastic properties of a general granitic crust. We test for two typical aquifer-types found in volcanic regions: unconsolidated pyroclastic deposits, commonly composed of coarse ash to fine lapilli sized clasts, and vesicular basaltic lava flows. These two types differ substantially in their elastic and fluid flow properties, which have significant influence on the observed signals. The layer above the aquifer, from here on called "cap rock", has elastic properties of a soft, impermeable clay. Input material properties for the reference simulation are given in Table 2; we used medians of parameter ranges found in the literature (Geotechdata.info, 2013; Freeze and Cherry, 1979; Wang, 2000; Adam and Otheim, 2013; Fetter, 1994; Gercek, 2007; Gudmundsson, 2011). Note that elastic properties of poroelastic layers are always required to be the drained parameters (i.e., measured under constant pore pressure). However, very few data exist on poroelastic parameters so we used the dry Young's

Moduli and Poisson's ratios instead and increased respective ranges in parametric sweeps to account for this unknown error. Within the different layers, material properties are considered isotropic and homogeneous. Standard water parameters are also given in Table 2.

2.3 Parametric studies and sensitivity analysis

In the parametric studies we investigated the effects of magmatic source properties as well as poroelastic and geometric properties of the aquifer (Table 2). When sweeping over one parameter, all others are kept constant. This entails that in all geometric sweeps, the distance between magma chamber top and aquifer was fixed, except for the sweep over magma chamber depth, because this distance is such an important parameter it would have otherwise overwhelmed the pure effects of, for example, aquifer thickness. When investigating the effects of magma chamber shape, we changed the horizontal half-radius b of an ellipsoidal chamber, which then defines the vertical half radius via the constant chamber volume. Pore fluid (H_2O) temperature was effectively changed by varying its density, viscosity and compressibility. We used the program provided by Verma (2003) to calculate these parameters for varying temperatures and a pressure of $4.5\mathrm{MPa}$, which represents average lithostatic pressure in the aquifer (Table 3). In a subset of simulations, the central portion of the aquifer is replaced with an area of zero permeability out to a radial distance L but with the same poroelastic properties as the aquifer, to avoid numerical errors at the inner boundary of the aquifer. Aquifer density and porosity have a negligible influence and have not been included in parametric study results.

To investigate the importance of parameters on hydraulic head change, we performed a sensitivity analysis. The influence of lateral distance L between magma chamber and aquifer onset has not been included in this analysis due to the lack of comparable signals (i.e., comparing the central hydraulic head change is not possible as the aquifer only starts at some radial distance) - it will be discussed in detail later. For each parameter value A with associated reference value A_{ref} we define $A* = \frac{A-A_{ref}}{A_{ref}}$, the fractional change of this parameter from its reference simulation value. To assess the sensitivity of head changes to changes in parameter values we plot the hydraulic head change, normalised by its value in the reference simulation, against $A*$. To account for the change in time and space, this has been done for different locations in the model domain and at different times during the simulation.

For both aquifers, plots as shown in Fig. 4 were produced for 4 different locations in the aquifer at 3 different simulation times, respectively. As the influence of many parameters varies in time and space, the ranking of parameters according to their significance is a two-step procedure. First, three parameter groups are defined based on the influence of a parameter on hydraulic head change in one individual plot (Table 4 and Fig. 4). Parameters are then ranked into 4 priority groups based on the number of plots in which they belong to a certain parameter group (Table 4). For example, a

parameter that changes hydraulic head to more than 2.5 times the reference value in more than 90% of the plots belongs to priority group 1.

2.4 Definition of nondimensional parameters

We also performed a dimensional analysis on the constitutive Eq. (1) to (6) as well as the boundary conditions of the model setup with a spherical chamber and L = $0\mathrm{km}$. Assuming constant pore fluid properties and aquifer thickness, this provided 11 nondimensional parameters that fully describe the system and can be grouped as follows:

Poisson's ratios of the three layers:

ν_c, ν_{aq}, ν_h

Coupling and fluid flow parameters:

The strength of the coupling between elastic deformation of the solid matrix and the pore fluid is crucial for hydraulic head changes that result from a compression or dilatation of the aquifer, as is the stiffness of the aquifer. This is expressed in the coupling parameter

$$\mathrm{Q} = \frac{\alpha}{\mathrm{SE}_{aq}}, \tag{9}$$

which determines how the aquifer can respond to the pressure changes. The Storage coefficient, S, informs how much water is released by (or stored in) the aquifer due to a fall (or increase) in pressure. The change in pressure in the simulated aquifer is determined by E_{aq} as the aquifer stiffness defines how it responds to magmatic strain. Therefore, the larger the product $\mathrm{S}{\cdot}\mathrm{E}_{aq}$, the more water gets released/stored and therefore the larger is the hydraulic head change. This relation is scaled by the Biot Willis coefficient, whose individual influence is quite complex as it is also included in the definition of S.

The flow parameter

$$F = \frac{\kappa}{\alpha d_{aq}^2} \tag{10}$$

determines how fast pressure can be distributed in the aquifer by relating the permeability - which determines flow velocity - to a length scale. This parameter is again scaled with the Biot-Willis coefficient.

Relative elastic properties:

A stronger pressurisation leads to a larger subsurface strain and therefore stronger poroelastic response. The aquifer Young's Modulus is an important factor for the poroelastic response and therefore used as a pressure scaling, leading to

$$\mathrm{ER}_l = \frac{\Delta P}{\mathrm{E}_{aq}} \tag{11}$$

as the nondimensional expression for loading of the chamber.

The stiffness of the host rock relative to aquifer stiffness

$$\mathrm{ER}_h = \frac{\mathrm{E}_h}{\mathrm{E}_{aq}}, \tag{12}$$

determines how strain changes at the boundary between host rock and aquifer - if the aquifer is stiffer than the host rock, the strain increases and vice versa.

$$\mathrm{ER}_c = \frac{\mathrm{E}_c}{\mathrm{E}_{aq}} \tag{13}$$

relates the stiffness of the cap rock to aquifer stiffness and determines how strain changes at the aquifer - cap rock boundary.

Geometry:

The distance of strain source to aquifer is determined by the scaled chamber depth

$$\mathrm{CD} = \frac{\mathrm{z}_T}{\mathrm{d}_{aq}} \tag{14}$$

and the scaled aquifer depth

$$\mathrm{AD} = \frac{\mathrm{z}_{centeraq}}{\mathrm{d}_{aq}}. \tag{15}$$

The scaled chamber radius

$$\mathrm{CR} = \frac{\mathrm{r}}{\mathrm{d}_{aq}} \tag{16}$$

contributes to the source strength.

Parametric sweeps were performed, varying one parameter group whilst all others were kept fixed. The parameter space (Table 5) was derived from ranges in dimensional sweeps and sometimes adapted as not all combinations of nondimensional parameters are physically reasonable. Note that, unlike in the dimensional sweeps, the distance between aquifer and magma chamber is not kept constant in the sweeps of the geometry group.

3 Results

3.1 Reference simulation

The described model was run for each aquifer type, using reference values of parameters given in Table 2, with a magma chamber pressurisation of $10\mathrm{MPa}$. In both aquifer types, the pressurisation of the magma chamber induces a fall in hydraulic head, which is strongest directly above the magma chamber and decreases with radial distance from the chamber (Fig. 2). At distances larger than

5km from the centre, the initial head change is of opposite sign compared to the central areas, but the amplitude of the head rise here is small in comparison with the central signal. There is also a comparatively small vertical gradient in the hydraulic head values. Whilst the pattern of the head change is the same in both aquifers, the absolute value of the signal differs substantially. In the pyroclastic aquifer, the maximum head fall is about 1.4cm, while the hydraulic head in the lava flow aquifer falls by a maximum of 6m. The initial hydraulic head change profile perfectly mirrors the strain curves (Fig. 2), illustrating that strain is the driver for the head changes. The aquifer is subject to dilation (positive strain), with a maximum value centrally above the chamber, which changes to compression (negative strain) with radial distance. Like for the hydraulic head, the two aquifers show similar patterns in strain, but different absolute values. Maximum volumetric strain in the pyroclastic aquifer is about 3 microstrain, while it is 13 microstrain in the lava flow aquifer.

Figure 3 illustrates the fluid flow pattern in the simulations, showing a strong fluid flow towards the centre, i.e. from higher to lower hydraulic head values following the pressure gradient. Flow speeds again demonstrate the very different behaviour of the two aquifer types, being an order of magnitude higher in the lava flow aquifer. Porous flow in the pyroclastic aquifer has a vertical component (down towards the magma chamber) but generally the lateral flow is predominant. Fluid flow is important because it equilibrates pressure in the aquifer and is responsible for the changes of strain and hydraulic head signals with time. Figure 3 shows the change with time of hydraulic head and volumetric strain, respectively, in a point in the aquifer centrally above the chamber. The hydraulic head tends towards zero with time; volumetric strain increases and evolves to an equilibrium non-zero value. Whilst time-dependent changes take place almost until the end of simulation duration (1000 days) in the pyroclastic aquifer, the values in the lava flow aquifer reach equilibrium after less than 10 days.

3.2 Sensitivity analysis

Exemplary plots used for the sensitivity analysis are shown in Fig. 4, demonstrating the significant differences in the individual influence of parameters. Following the definitions of the priority groups we can rank the investigated parameters as follows:

- Priority 1: aspect ratio and volume of the chamber.
- Priority 2: Biot-Willis-coefficient, temperature of the pore fluid and depth of the chamber.
- Priority 3: Young's Modulus and permeability of the aquifer and chamber pressurisation value.
- Priority 4: Poisson's ratio, depth and thickness of the aquifer.

This ranking is, however, only a relative one - even those parameters of the last priority group have a non-negligible influence on the resulting hydraulic head change. Furthermore, the ranking of a parameter depends partly on the range of values tested for that parameter. This is particularly

important in interpreting the sensitivity to the Biot-Willis-coefficient (α). Due to the scarcity of experimental data for this parameter, the sweeps in both aquifer cases were performed over the whole mathematical range of α between the porosity and 1. However, the true value of α for natural soft rocks should be close to 1, while it is close to the porosity for hard rocks. Therefore, although ranked here as priority 2, in reality the Biot-Willis-coefficient might belong in a lower priority group. More information on the individual influence of α can be found in Appendix B.

3.3 Results of parametric studies

The dimensional and nondimensional parametric sweeps provided a number of interesting insights, we are focusing here on describing the most important ones.

3.3.1 Influence of material properties

Figure 5 shows the influence of the coupling parameter Q and the flow parameter F. Generally, a larger Q means a weaker pressure response of the aquifer to applied strain from the chamber pressurisation and hence leads to a smaller hydraulic head change. For example, the reference value of Q in the pyroclastic aquifer of 4.89 corresponds to a hydraulic head fall of $1.4\mathrm{cm}$; if Q is decreased by 3 orders of magnitude, the central hydraulic head changes by several meters (see Fig. 5a). Porous flow in the aquifers decreases hydraulic head signals with time. As F determines porous flow it does not have any influence on the initial head signal. But a larger F leads to a smaller remaining central hydraulic head change after some time passed, because quicker porous flow leads to a faster equilibration of pore pressure in the aquifer. Figure 5b shows that for the largest value of F in the lava flow aquifer (5×10^{-14}), the remaining central hydraulic head change is negligible after just 1 day, while it still equals the initial value for a small value of F (5×10^{-18}).

It is common that aquifers are heated in volcanic settings. Figure 6 shows the substantial influence of changing the pore fluid temperature on the initial hydraulic head change and its evolution with time, especially when temperatures are above the pressure-dependent boiling point and the aquifer pores are no longer filled with liquid water, but steam. With increasing temperature of liquid water, the initial hydraulic head change is reduced in the lava flow aquifer, whereas it is very slightly increased in the pyroclastic aquifer (Fig. 6). For steam-filled pores (above $300^\circ\mathrm{C}$), the initial central hydraulic head change in the pyroclastic aquifer is an order of magnitude larger than for liquid water - in the lava flow aquifer the opposite relation is true. Interestingly, the order of magnitude of hydraulic head change is the same in the two different aquifer types when steam saturated, while there is a two order of magnitude difference in the signals for the water saturated aquifers. In both aquifers, hydraulic head change increases with increasing temperature of the steam. Additionally, porous flow is much slower in the steam-aquifers compared to water-aquifers.

Of the aquifer's elastic properties, namely the Poisson's ratio and the Young's Modulus, only the latter is significant for the poroelastic response to applied strain. Not only is the absolute stiffness

of the aquifer important, but also its value relative to the surrounding lithology and pressurisation of the chamber. We therefore present these results using the nondimensional parameters ER_l, ER_h and ER_c. There is a linear relationship between the relative loading (or decompression) of the chamber ER_l and hydraulic head change. To collapse the curves for different ER_l values, we plot the ratio $\frac{\Delta h}{\mathrm{ER}_l}$ against ER_c for different ER_h values in Fig. 7. Figure 8b shows vertical strain profiles from $2\mathrm{km}$ depth to the surface for different stratigraphies, illustrating how strain changes at the boundary between different elastic mediums: strain increases when hitting a stiffer medium and vice versa.

ER_h determines this change at the host rock - aquifer boundary. A larger ER_h indicates an aquifer softer than the host rock and therefore results in a smaller strain in the aquifer and hence smaller hydraulic head change (Fig. 7). The relative cap rock stiffness ER_c determines the strain change at the aquifer - cap rock boundary and has negligible influence when it is small ($\mathrm{ER}_c < 0$). However, it becomes increasingly important when the cap rock stiffness is close to or larger than that of the aquifer ($\mathrm{ER}_c > 1$): Figure 7 shows how a stiff caprock can decrease the hydraulic head change and even change its sign. This "sign-flipped" signal increases with larger ER_c, as can be seen for the pyroclastic aquifer for ER_c values larger than 100 (Fig. 7a).

Figure 8a shows the hydraulic head change along a horizontal profile in a sign-flipped aquifer. In contrast to the reference case, the central head change here is positive and changes sign twice: at about $3\mathrm{km}$ radial distance to a fall, and again at about $6\mathrm{km}$ to a head rise - mirroring sign-flipped volumetric strain. This change in sign is due to the strain jump at the host rock - aquifer boundary, which is also influenced by ER_c: in the sign-flipped case, the dilatational strain in the host rock is turned into compression in the aquifer. Figure 8b shows this very different strain profile of a sign-flipped case due to a large ER_c value in comparison to the reference situations.

By sweeping ER_c of the pyroclastic aquifer together with sweeping all other nondimensional parameters, we found that the ER_c value at which the strain sign is flipped ("ER_{cflip}") is determined by the geometry of the system, in particular by the depths of aquifer and magma chamber. For a deeper aquifer, ER_{cflip} is smaller, while a deeper magma chamber leads to a larger ER_{cflip}.

3.3.2 Influence of the geometry

We use the nondimensional parameters AD (scaled aquifer depth), CD (scaled chamber depth) and CR (scaled chamber radius) to demonstrate combined geometric effects. For different chamber radii, we plot initial hydraulic head change versus the nondimensional distance between magma chamber and aquifer, CD-AD, in Fig. 9. The larger the chamber radius the larger is the resulting hydraulic head change in the aquifers. For the lava flow aquifer the magma chamber depth has no influence on hydraulic head change as long as the distance between aquifer and magma chamber is constant. The individual curves for different chamber depths can be easily connected to one curve showing the dependance of hydraulic head on CD-AD (9b and d). The smaller this distance, the larger is the hydraulic head fall.

This relation is somewhat more complicated for the pyroclastic aquifers, where hydraulic head depends on the distance between chamber and aquifer but also on the chamber depth. The central hydraulic head in the pyroclastic aquifers (Fig. 9a) is positive (hence sign-flipped) for sufficiently small distance between aquifer and chamber, then switches sign to a head fall at a value $(CD-AD)_{flip}$ and increases with further increasing distance. The value $(CD-AD)_{flip}$ is larger, the deeper the chamber. Extrapolating the curves for different chamber depths indicates that central hydraulic head change is larger for deeper chambers, if hydraulic head change is positive. If the hydraulic head change is negative then it is larger for shallower chambers. The relationship at $2\mathrm{km}$ radial distance from the center (Fig. 9c) also depends on both chamber depth and distance to aquifer. For the shallowest chamber (CD=10), the (negative) hydraulic head change first decreases with increasing distance between aquifer and magma chamber, then reaches a minimum and starts increasing again (CD=5 simulations show a similar relationship, although not testable with all CR and AD values, as chamber and aquifer come too close). The other tested chamber depths show similar relationships as seen for the central hydraulic head change, although the tested CD-AD values are not small enough to cause sign-flipped hydraulic head changes. Normally, the maximum hydraulic head fall is directly above the chamber. However, when considering a hydraulic head profile through the pyroclastic aquifer for a shallow magma chamber without a sign-flipped strain (i.e., CD=5 and AD=AD$_{ref}$, see Appendix C), the maximum head change is no longer central but laterally offset by up to $1\mathrm{km}$.

We also evaluated the influence of the shape of the magma chamber by incorporating tests for a prolate and oblate spheroid. Although chamber volumes are constant, the shape can change the hydraulic head signal by an order of magnitude. Figure 10 shows that the amplitude is highest for oblate chambers, intermediate for a sphere and smallest for prolate chambers.

Instead of having an "infinite" aquifer covering the whole volcano, we also varied the lateral distance L between the centre of the model and the onset of the aquifer, realised by a zero permeability zone in the centre of the domain (compare Fig. 1). The initial hydraulic head in these shorter aquifers equals the respective value at the same location in the reference aquifer. After some time, however, the head signal in the shorter aquifer differs substantially from the reference case. Figure 11 shows the remaining head changes after 10 days of simulation in the pyroclastic aquifer and after 1 day in the lavaflow aquifer, respectively (the different timescales were used to account for the faster processes in the latter case). Compared to the profile of hydraulic head in the reference simulation, remaining maximum head changes in aquifers starting at $2\mathrm{km}$ radial distance are considerably smaller (about 50% in the pyroclastic aquifer and 66% in the lava flow aquifer). This difference is strongest close to the lateral aquifer boundary facing the domain center - with radial distance, the head change profile of the shorter aquifer approximates the reference profile. In the case of the pyroclastic aquifer, the difference between reference and shorter aquifer is negligible after the first kilometer, while in the lavaflow aquifers head values differ considerably from each other over much longer distances.

The pyroclastic aquifer starting at $4\mathrm{km}$ distance also shows a smaller remaining head change than the reference case, while the more distant aquifers are almost non-distinguishable from the reference case on a centimeter scale. Lava flow aquifers starting at $4\mathrm{km}$ or further radial distance however are all significantly different from the reference case and show positive head changes (up to $10\mathrm{cm}$), while the reference aquifer at this time shows negative values everywhere less than about $10\mathrm{km}$ radial distance from the centre.

Figure 12 shows the different flow patterns in the first $8\ \mathrm{km}$ of 3 different aquifers after 0.1 days of simulation. For $\mathrm{L} = 8\mathrm{km}$ (topmost aquifer in the figure), the aquifer shows a completely reversed flow pattern compared to the reference case. Instead of flowing towards the centre, water flows away from it. The pyroclastic aquifer shows a strong downward component of the flow as well, but develops a laterally dominated flow pattern at later simulation times. For $\mathrm{L} = 2\mathrm{km}$ (bottom aquifer in Fig. 12), the aquifer shows a flow pattern similar to the reference simulation, while two flow directions can be observed for $\mathrm{L} = 6\mathrm{km}$ (middle aquifer in Fig. 12) - one towards and one away from the volcano. At later simulation times, the flow towards the volcano diminishes and then all flow is away from the centre of the domain. Generally, the shorter aquifers show lower flow velocities than the longer ones.

4 Discussion and Implications

4.1 Model limitations

In order to investigate poroelastic aquifer responses to crustal deformation, we made some simplifying assumptions. For one, the presented models only consider single-phase, single-component flow under constant temperature conditions. However, our parametric studies have shown that the pore fluid properties significantly influence the resulting head changes. Hydrothermal systems can contain steam, water and a number of solutes, and temperatures can change substantially. Additionally, the injection of the hydrothermal fluids into the aquifer can lead to pore pressure increase, heating and further deformation (see e.g. Fournier and Chardot (2012) for a one-way-coupled model). We focused on the pure poroelastic response, but the poroelastic, heating and phase change processes superimpose each other.

Secondly, the aquifer was fully saturated and confined. To keep this study feasible, we did not investigate unconfined aquifers as this would imply a non-saturated permeable zone, and the coupling of linear elastic behaviour with non-saturated porous flow is associated with a high computational effort and often the solvers fail to converge due to the high nonlinearity of the problem.

The discussed models are most applicable to confined aquifers that do not undergo extensive heating during the observation period (e.g., aquifers at some distance of the volcanic centre). They present a good opportunity to better understand poroelastic aquifer responses that have been used for monitoring. Their advantage over previous models is the full 2-way coupling of flow and linear

elastic behaviour and that we are able to simulate various geometries. The comparatively short computation time (on the order of 5 to 10 minutes per simulation depending on geometric complexity and number of necessary time steps) allows the study of a large number of parameters and their influence on hydraulic head changes and flow pattern.

4.2 General aspects

Our simulations show that no injections of fluids or fracture flow is needed to induce hydraulic head changes of several metres in an aquifer. Volumetric strain induced by a magma chamber pressurisation causes hydraulic head changes in local aquifers. Dilation above the chamber, due to ground uplift, leads to a fall in pore pressure, while the accompanying compression in lateral distance from the centre of the uplift induces a head rise. Poroelastic processes are therefore a reasonable approach to interpret large water level changes observed at volcanoes. For the same source and model geometry we could observe large differences between the two typical aquifer types. These differences are mainly due to the different elastic properties of the aquifers: the pyroclastic aquifer is much softer than the lava flow aquifer and therefore strain attenuation is stronger, hence the resulting hydraulic head change is smaller.

The induced pressure gradient in the aquifers induces porous flow which leads to temporal changes in hydraulic head and strain. Fluid flow velocity is determined by the permeability of the porous medium and magnitude of the pressure gradient, which explains the difference between the two aquifers. Flow is faster in the lava flow despite having an order of magnitude lower permeability because the pressure gradient is two orders of magnitude larger than in the pyroclastic aquifer. The higher permeability in the pyroclastic aquifer allows a non-negligible component of the flow to follow the comparatively small vertical pressure gradient in the aquifer. The hydraulic head tends towards zero with time because pressure in the aquifer is equilibrated by the flow. The equilibrium strain value represents the strain value in an elastically equivalent, but dry material, because the initial stress absorption by the pore fluid (final term in Eq. (2)) vanishes with pressure equilibration. Stress absorption of the fluid leads to an initial strain reduction by a factor of 4 in the pyroclastic aquifer, while it is negligible in the lava flow aquifer due to its smaller Biot-Willis-coefficient.

The above findings highlight the necessity of a full coupling of fluid and solid mechanics. Both the effect of ground deformation on the pore fluid, as well as the influence of a pore fluid on strain in the solid matrix need to be considered to fully understand well level and/or strain signals.

Parametric studies have shown that poroelastic aquifer responses are complex processes that are strongly influenced by source, geometrical and aquifer parameters as well as the elastic stratigraphy. Chamber radius and pressurisation determine the strength of the deformation source and the subsurface strain it causes. Strain partitioning in the crust is regulated by the elastic properties of the different layers. A special case occurs when the caprock is sufficiently stronger than the aquifer. The stiff caprock prevents the dilatation of the aquifer and turns the strain into compression, hence

causing sign-flipped signals. The subsurface stress and strain field is also substantially dependent on the shape of the chamber. For oblate chambers, the aquifer area that is exposed to vertical stress is larger than for prolate chambers and it is therefore subject to stronger strain. The distance between aquifer and magma chamber is another factor contributing to the strength of the strain field affecting the aquifer. Generally, the closer the aquifer to the source, the stronger is the strain and hence its pressure response. However, if elastic properties are close to values causing a sign-flipped signal, a sufficiently close aquifer-source distance can lead to a sign-flipped strain (because ER_{cflip} is changed) and hence sign-flipped hydraulic head change in the aquifer.

The elastic properties of the solid matrix as well as the pore fluid together with the Biot-Willis coefficient of the aquifer determine the initial pressure response of the aquifer to the strain changes. Flow properties then determine the velocity of pressure equilibration and therefore the development of head and strain signals with time. Of particular interest is the influence of pore fluid temperature. It can change the hydraulic head response by an order of magnitude as well as influence the flow behaviour in the aquifer. This is especially important in volcanic environments, where heat flow is high and therefore temperature changes are likely. Changing the temperature means changing compressibility, density and viscosity of the water. By testing simulations with changing only one of the three parameters, we could distinguish their individual influence. The viscosity does not influence the initial head value, but determines the speed of equilibration, which is faster for liquid water than for steam (compare Eq. (5)). Decreasing the density of the pore fluid increases the hydraulic head change, while increasing the compressibility decreases it. With increasing temperature and phase change to steam, we therefore see a combination of these two effects. In the pyroclastic aquifer, the density effect dominates, while in the lava flow aquifer the compressibility effect is more important. While we investigated the temperature effect, other processes could also change pore fluid properties, such as dissolved minerals, and thereby play a role in determining the hydraulic head change.

Porous flow in the aquifer and therefore evolution of signals with time is also significantly influenced by the lateral distance between the magma chamber and the aquifer, even though initial hydraulic head values at respective locations are the same. Generally, the initial hydraulic head is negative in the first $5\mathrm{km}$ of lateral distance from the centre and is positive more distally; this pressure profile causes flow towards the center. However, if the aquifer onset falls in the "positive head"-area, the driving pressure gradient and hence flow is reversed. For aquifers that onset near the transition zone, two flow directions can be observed - one towards and one away from the centre of the volcano. These two directions are due to the maximum initial head change being not directly at, but lateral offset from the lateral aquifer boundary. This can be seen in the profile of the initial hydraulic head change in the reference simulations: beyond $5\mathrm{km}$ from the center, hydraulic head change first increases with distance before decreasing again. While this comparatively small gradient is negligible in the reference simulation, as flow is dominated by the much stronger gradient towards the centre, it matters for flow in aquifers that start close to the transition zone from positive to negative strain.

The differences in remaining hydraulic head changes in the aquifers starting at varying distances are due to these different flow processes caused by the changed initial pressure gradients.

4.3 Implications for volcano monitoring

The strain sensitivity of an aquifer is the change of hydraulic head in meters per unit applied strain. As the simulated initial hydraulic head change mirrors the volumetric strain, our models suggest that an accurately determined strain sensitivity can indeed be used to infer volumetric strain in the aquifer from measured water level changes. Figure 13 shows the theoretical strain sensitivity of the two aquifers used in the reference simulation, determined by dividing the simulated hydraulic head change by the volumetric strain. This has been done along profiles through the aquifers. The very small strain and head values close to the transition zone from dilatational to compressional strain lead to numerical errors in the determined strain sensitivities in these locations (which can be reduced by increasing the mesh density), but in general we calculate a consistent value. Strain sensitivity of the pyroclastic aquifer is about -5$\times 10^3$m; the lava flow aquifer has a strain sensitivity about 2 orders of magnitude larger.

However, the influence of flow on strain sensitivity is problematic; Fig. 14 shows a decrease of theoretically calculated strain sensitivity with time, which is comparable to the decrease of the hydraulic head change. Hence, the strain sensitivity value determined from aquifer responses to known strains only provides accurate strains when applied to the initial hydraulic head change, as it does not take flow processes into account. Due to the necessity of knowing the initial hydraulic head response to use strain sensitivity, information about flow in the aquifer is important. The acquisition of permeability data, e.g. via pumping tests, should be part of hydrological monitoring efforts as it can help decipher flow processes. In any case, observing the flow behaviour in the aquifers, by installing several observation wells, can be a valuable addition to existing monitoring efforts as they could reveal flow patterns associated with strain-induced head change. Additionally, it is important to know aquifer geometry as the models show that the flow pattern strongly depends on the lateral distance from the aquifer to the source.

Our parametric studies show how poroelastic aquifer responses are influenced by a variety of source, geometrical and aquifer parameters, which each have the potential to significantly alter the signal amplitude and development with time and space. Consequently, a change in any of these parameters could lead to a change in an observed hydraulic head. In addition, the porous flow alters the initial hydraulic head signal with time. Therefore not all observed aquifer pressure transients are necessarily related to a change in the magmatic system, which needs to be carefully considered when interpreting observed water level changes.

Even if strain sensitivity has been accurately used to infer volumetric strain, we still face the problem of interpretation of this signal. To invert for the source of strain, it is very common to assume a source in a homogeneous half space. Additionally, some models only consider spherical chambers

and all previous approaches treated their data as a result of dry deformation. Our results underline that any model using these simplifications will likely be inadequate when used for interpretation of poroelastic processes. Firstly, chamber shape is one of the two most important parameters influencing the signal. Therefore, the assumption of a spherical chamber is a likely source for substantial mistakes and several chamber shapes have to be tested. But even if chamber shape is taken into account, the assumptions of a homogeneous half space and dry deformation can lead to further misinterpretation.

The stress absorption of a pore fluid leads to a reduction of initial strain in the aquifer when compared to an elastically equivalent, dry layer. If the initial strain is used to infer the magmatic source based on a model for dry deformation, its strength can be underestimated, as this stress reduction is not taken into account. One therefore faces the dilemma of needing the "dry" equilibrium strain for correct application of any dry deformation model but only having a tool (i.e., strain sensitivity) to determine initial strain from the initial head response. However, "dry" strain is reached in the aquifer after porous flow has equilibrated the pressure. So, this problem could be solved when permeability data and sufficiently dense time series of hydraulic head data are available: strain sensitivity can be combined with the evolution of signals with time to infer initial as well as equilibrium "dry" strain. This emphasises again the need for acquiring accurate data on hydrological conditions.

The third assumption of a homogeneous half space is precarious as volcanoes are strongly heterogeneous, which is particularly emphasised by the presence of a confined aquifer. The investigation of the elastic stratigraphy has shown that hydraulic head change and consequently derived strain strongly depend on heterogeneities and might not at all be what would be expected from a source in a homogeneous crust. Especially in settings with a strain-flipped signal, i.e. where the dilatational strain in the aquifer is turned into compression by a stiff caprock, this influence becomes crucial. The hydraulic head rises and hence interpretation of the hydraulic head data alone would suggest a deflating chamber, while it is really inflating. We simulated ground deformation signals with the aim to investigate whether they - if available - could aid with this problem. Figure 15 shows the central hydraulic head and surface displacement signals with time for the pyroclastic aquifer with two different cap rocks: a soft one (E_c = 10MPa) and a stiff one (E_c = 10GPa), hence different ER_c values. The latter leads to a change of sign of the volumetric strain and thereby to a positive hydraulic head change as opposed to a fall in the first case. The surface deformation however does not change sign and shows inflation of the ground in both cases and can hence be used to indicate that the strain in the aquifer is sign-flipped. Additionally, we can observe a different time dependent behaviour. In the normal case with no sign-flipped strain, the negative hydraulic head leads to an initial strain-reduction in the aquifer. If the strain sign is changed in the aquifer and the hydraulic head change is positive, strain and displacement in the aquifer is increased compared to the non-coupled case. Both phenomena - stress-absorption and stress-addition - decrease with time due to equilibration of pore pressure in the aquifer and hence ground deformation increases for an initial negative head, whilst

it decreases if the initial head was positive. The change of ground deformation with time in this case will be below the detection limit, but could be larger for certain scenarios. Therefore, if we are able to observe ground deformation and hydraulic head with time, this helps to infer the true strain distribution in the subsurface.

In summary, while water level data can be a valuable addition to monitoring systems and be a cheaper replacement for strainmeters, one needs to be careful when interpreting the data. We need to take into account that many parameters influence the water level changes and that most of the commonly used analytical dry deformation models might fail to explain the observations.

4.4 The Usu 2000 water level changes revisited 

The above considerations provide several possible scenarios to explain the apparent inconsistency of well data in the the 2000 Usu case (Matsumoto et al., 2002), where only one of the two observed well water level changes agrees with the proposed model. If strain sensitivities determined by Matsumoto et al. (2002) are correct and time series qualities are of sufficient quality to provide initial head changes, then the strains they derived are accurate. But the strain data from each well appear to give very different information about the source: estimated volumes differ by a factor of three. Only the well slightly farther away from the volcano, which points to the smaller source, agrees with ground deformation data from a GPS station closer to this well. Even if there are errors in the determination of strain we expect they would be similar for both wells, and the question of the disagreement in source information remains. The authors applied the Mogi model to invert for the source, hence assuming a spherical source in a homogeneous, dry half space. We can suggest four possible explanations:

- The source is not spherical: an oblate chamber leads to a larger signal gradient and could therefore explain a larger signal closer to the source while it still holds for the smaller signal at the more distal well.
- The subsurface is heterogeneous: the two aquifers - although having similar coupling properties - are surrounded by different lithologies that increased the strain in the closer aquifer.
- The aquifers have different Biot-Willis-coefficients: strain reduction in the distant aquifer is sufficiently large (i.e., this aquifer has a large α) such that the "true" dry strain and therefore the source is underestimated, while α of the closer aquifer is smaller and the derived strain is therefore closer to its dry value.
- The problem is flow-related: the observed water level rise occurred over the course of 2-3 days (not instantaneous pressurisation of the system). If F of the distant aquifer is large enough, the accumulated final rise here does not represent the total strain increase, as some pressure increase would be already equilibrated by flow during the rise-period. If F in the closer aquifer is smaller, this effect is smaller and more initial hydraulic head change remains.

A corollary of the last two scenarios is that the signal from the close well should be the most reliable, which is inconsistent with the agreement between the GPS data and the more distal well. It is therefore more likely that the assumptions of a spherical source and/or a homogeneous crust are the reasons for the apparent discrepancy between model and observations.

5 Conclusions

In this study we presented fully-coupled numerical models to investigate the interaction between solid mechanics and fluid flow in porous media. We have shown that strain changes due to the inflation of a magma chamber lead to significant hydraulic head changes and porous flow in the local hydrology. The flexibility of the Finite Element Analysis method allowed us to perform extensive parametric studies providing detailed insights in these poroelastic processes. Parameters controlling aquifer behaviour are in order of importance (i) the shape and volume of the magma chamber (ii) depth of the magma chamber and state of the pore fluid (iii) chamber pressurisation value, Young's Modulus and permeability of the aquifer. Magmatic source properties and distance between chamber and aquifer determine the strain field; strain partitioning is defined by elastic stratigraphy of the crust. Coupling and flow parameters of the aquifer define its response to this strain and how head and strain signals change with time due to porous flow.

One aim of this study was to investigate the accuracy of the method to combine strain sensitivities with deformation models to interpret observed hydraulic head changes. Our models show that volumetric strain in the aquifer can indeed be inferred from hydraulic head changes using strain sensitivities, under two conditions. Firstly, one needs to account for flow processes by either making sure to measure the initial hydraulic head change or use a known permeability to extrapolate it; this can also be achieved with dense time series of head data. Secondly, we need to ensure that strain sensitivities have been accurately determined and not changed with time due to changes in the hydrology.

However, using common analytical deformation models for the interpretation of this strain information is problematic, as several assumptions of these models can lead to substantial misinterpretation. They are only applicable for a comparatively homogeneous crust (i.e., $E_{aquifer} \approx E_{cap} \approx E_{host}$), when one either accounts for fluid induced strain reduction or considers an aquifer with very little strain reduction. The shape of the chamber needs to be taken into account as well.

The hydraulic head signal is very sensitive to source volume, shape, depth and pressurisation value. This suggests that if we know the aquifer coupling and flow parameters, some information about the source can be gained from hydraulic head changes - although solutions will always be non-unique. Our analysis has shown the necessity of numerical models to account for the large number of parameters that significantly influence the results. Nevertheless, well water level changes can be interpreted as poroelastic responses to subsurface strain changes and aquifers can serve as

comparatively cheap strain meters, especially if data on flow properties and hydrological geometry are available. They therefore are a valuable complement to other monitoring systems.

Appendix A: Benchmarking

We compared a numerically derived solution to a known analytical solution. The benchmarking problem is known as "Terzaghi's compaction": a homogeneous poroelastic block is compressed by applying a load to its upper surface. The analytical solution provides expressions for the pore pressure as well as solid displacement in time and space (e.g., Wang, 2000)). We simulated a 2D domain in COMSOL with measurements of 10×10km and the following boundary conditions: rollers at the lateral boundaries, fixed bottom boundary and a loaded surface; no flow outside the domain. In general, numerical and analytical solution show a good agreement (Fig. A1), except for the solution for pore pressure at 100m depth, where the numerically calculated value oscillates slightly and varies from the analytical solution for the first 0.2 seconds of the simulation (Fig. A1d). The largest difference is about 2% and due to numerical instability at a small distance to the applied boundary load. However the error becomes negligible after 0.1 days and can be easily reduced with increasing mesh density close to this boundary.

Appendix B: Biot-Willis-coefficient

The influence of the Biot-Willis coefficient is quite complex, as it defines the coupling terms in the constitutive equations and is involved in the definition of storativity of the aquifer as well. Figure B1 shows the effect of varying the coupling parameter on the initial central hydraulic head change for the two different aquifer types. In the pyroclastic aquifer, the head fall first strongly decreases with increasing α, then reaches a plateau at α=0.6, which is followed by a very steep increase of head fall when the Biot-Willis coefficient approaches 1. In the lava flow aquifer, the hydraulic head change is larger for larger α.

The steep decrease of Δh for α approaching 1 for the pyroclastic aquifer can be mathematically explained by considering an order of magnitude analysis of the definition of the storage coefficient (Eq. 6):

$$\begin{aligned} S &= \phi\chi_f + \frac{(\alpha-\phi)(1-\alpha)}{\mathrm{K}} \\ &= \phi\chi_f + \frac{(\alpha-\phi)(1-\alpha)3(1-2\nu)}{\mathrm{E}} \\ &\approx 10^{-1}\times10^{-10} + \frac{10^{-1}\times(1-\alpha)*10^{0}\times10^{-1}}{10^{7}} \text{(for the pyroclastic aquifer)} \\ &= 10^{-11} + 10^{-9}\times(1-\alpha) \end{aligned}$$

So, in the pyroclastic aquifer for $\alpha \leq 0.9$, $\phi\chi_f$ is one order of magnitude smaller than the right summand, which therefore dominates the definition of S. But for $\alpha = 1$, S equals $\phi\chi_f$. Therefore,

there is a steep change of S between $\alpha = 0.9$ and $\alpha = 1$. For the lava flow aquifer, E$\approx 10^{10}$ and therefore the right summand has the order of magnitude $10^{-11} \times (1 - \alpha)$ and $\phi\chi_f$ is the dominating term in the definition of S for all α. This is also the explanation for the different dependance of Δh on α for the two aquifers. In the pyroclastic aquifer, changing α changes the coupling terms and the storage coefficient, while in the lava flow aquifer changing α has almost no effect on S.

Appendix C: Extra information on the influence of chamber depth

For a shallow magma chamber, in a situation with nosign-flipped strain, the maximum head change in the pyroclastic aquifer is no longer central, but laterally offset by up to $1\mathrm{km}$ (shown for CD=5 and AD=AD$_{ref}$ in Fig. C1).

Acknowledgements. The research leading to these results has received funding from the People Programme (Marie Curie Actions) of the European Union's Seventh Framework Programme (FP7/2007-2013) under the project NEMOH, REA agreement n° 289976. Additional funding was provided by the MED-SUV project, under grant agreement n° 308665, and the VUELCO project under grant agreement n° 282759, both part of the European Union's Seventh Framework Programme.

References

Adam, L. and Otheim, T.: Elastic Laboratory Measurements and Modeling of Saturated Basalts, J GEOPHYS RES - SOL EA, 118, 840–851, 2013.

Bonaccorso, A., Calvari, S., Linde, A., Sacks, S., and Boschi, E.: Dynamics of the shallow plumbing system investigated from borehole strainmeters and cameras during the 15 March, 2007 Vulcanian paroxysm at Stromboli volcano, EARTH PLANET SC LETT, 357-358, 249–256, 2012.

Chiodini, G., Caliro, S., De Martino, P., Avino, R., and Gherardi, F.: Early signals of new volcanic unrest at Campi Flegrei caldera? Insights from geochemical data and physical simulations, GEOLOGY, 40, 943–946, 2012.

COMSOL: COMSOL Subsurface Flow Module User's Guide, Version 4.4, COMSOL, 2013.

Davis, E., Wang, K., Thomson, R., Becker, K., and Cassidy, J.: An episode of seafloor spreading and associated plate deformation inferred from crustal fluid pressure transients, J GEOPHYS RES, 106, 21 953–21 963, 2001.

Fagents, S., Greggs, T., and Lopes, R., eds.: Modeling Volcanic Processes, The Physics and Mathematics of Volcanism, Cambridge University Press, 2013.

Fetter, C.: Applied Hydrogeology, Macmillan Company, New York, 1994.

Fournier, N. and Chardot, L.: Understanding volcano hydrothermal unrest from geodetic observations: Insights from numerical modeling and application to White Island Volcano, New Zealand, J GEOPHYS RES - SOL EA, 117, 2012.

Freeze, R. and Cherry, J.: Groundwater, Prentice-Hall, Englewood Cliffs, N.J, 1979.

Geotechdata.info: Soil Young's Modulus. http://geotechdata.info/parameter/soil-elastic-young-modulus.html, http://geotechdata.info/parameter/soil-elastic-young-modulus.html, 2013.

Gercek, H.: Poisson's ratio values for rocks, INT J ROCK MECH MIN, 44, 1–13, 2007.

Gudmundsson, A.: Rock fractures in geological processes, Cambridge University Press, 2011.

Hickey, J. and Gottsmann, J.: Benchmarking and developing numerical Finite Element models of Benchmarking and developing numerical Finite Element models of volcanic deformation, J VOLCANOL GEOTH RES, 280, 126–130, 2014.

Jonsson, S., Segall, P., Pedersen, R., and Björnsson, G.: Post-earthquake ground movements correlated to pore-pressure transients, NATURE, 424, 179–183, 2003.

Linde, A. T., Sacks, S., Hidayat, D., Voight, B., Clarke, A., Elsworth, D., Mattioli, G., Malin, P., Shalev, E., Sparks, S., and Widiwijayanti, C.: Vulcanian explosion at Soufrière Hills Volcano, Montserrat on March 2004 as revealed by strain data, GEOPHYS RES LETT, 37, 2010.

Matsumoto, N., Sato, T., Matsushima, N., Akita, F., Shibata, T., and Suzuki, A.: Hydrological anomalies associated with crustal deformation before the 2000 eruption of Usu volcano, Japan, GEOPHYS RES LETT, 29, 1057, 2002.

Mogi, K.: Relations between the eruptions of various volcanoes and the deformations of the ground surfaces around them, B EARTHQ RES I TOKYO, 36, 99–134, 1958.

Newhall, C., Albano, S., Matsumoto, N., and Sandoval, T.: Roles of groundwater in volcanic unrest, Journal of the Geological Society of the Philippines, 56, 69–84, 2001.

Roeloffs, E.: Poroelastic techniques in the study of earthquake-related hydrologic phenomena, ADV GEOPHYS, 37, 135–195, 1996.

Shibata, T. and Akita, F.: Precursory changes in well water level prior to the March, 2000 eruption of Usu volcano, Japan, GEOPHYS RES LETT, 28, 1799–1802, 2001.

Shibata, T., Matsumoto, N., Akita, F., Okazaki, N., Takahashi, H., and Ikeda, R.: Linear poroelasticity of groundwater levels from observational records at wells in Hokkaido, Japan, TECTONOPHYSICS, 483, 305–309, 2010.

Stefansson, V.: Geothermal Systems: Principles and Case Histories, chap. The Krafla geothermal field, pp. 273–294, Wiley, New York, 1981.

Takahashi, H., T., S., Yamaguchi, T., R., I., Okazaki, N., and Akita, F.: Volcanic strain change prior to an earthquake swarm observed by groundwater level sensors in Meakan-dake, Hokkaido, Japan, J VOLCANOL GEOTH RES, 215, 1–7, 2012.

Verma, M.: Steam tables for pure water as an ActiveX component in Visual Basic 6.0, Computers and Geosciences, 29, 1155–1163, 2003.

Voight, B., Linde, A. T., Sacks, I. S., Mattioli, G. S., Sparks, R. S. J., Elsworth, D., Hidayat, D., Malin, P. E., Shalev, E., Widiwijayanti, C., Young, S., Bass, V., Clarke, A., Dunkley, P., Johnston, W., McWorther, N., Neuberg, J., and Williams, P.: Unprecedented pressure increase in deep magma reservoir triggered by lava-dome collapse, GEOPHYS RES LETT, 33, 2006.

Wang, H. F.: Theory of Poroelasticity with Applications to Geomechanics and Hydrogeology, Princeton University Press, 2000.

Table 1. Symbols

$\boldsymbol{u}$	Displacement [m]	b	Horizontal half-radius of ellipsoidal chamber [m]
σ	Stress tensor [Pa]	z_{aq}	Depth of aquifer top [m]
$\mathbf{F}_V$	Body Force [N]	$z_{centeraq}$	Depth of aquifer center [m]
ϵ	Strain [1]	d_{aq}	Thickness of aquifer [m]
ϵ_{vol}	Volumetric strain [1]	F	Nondimensional fluid flow parameter [1]
g	Gravitational constant [ms^{-2}]	Q	Nondimensional coupling parameter [1]
t	Time [s]	ER_l	Nondimensional loading [1]
p_f	Fluid pore pressure [Pa]	ER_h	Nondimensional host rock strength [1]
h	Hydraulic head [m]	ER_c	Nondimensional cap rock strength [1]
Δh	Hydraulic head change [m]	ER_{cflip}	ER_c-value that changes sign of strain in the aquifer [1]
$\boldsymbol{v}$	Fluid flow velocity [$ms-1$]	CD	Nondimensional chamber depth [1]
S	Storage [Pa^{-1}]	CR	Nondimensional chamber radius [1]
Q	Source/Sink [$kgm^{-3}s-1$)]	AD	Nondimensional aquifer depth [1]
ρ_f	Density of pore fluid [kgm^{-3}]	AD_{flip}	AD-value that changes sign of strain in the aquifer [1]
μ	Viscosity of pore fluid [Pas]		
χ_f	Compressibility of pore fluid [Pa^{-1}]		
T_f	Temperature of pore fluid [°C]		
C	Drained Elasticity Tensor [Pa]		
Φ	Porosity of the aquifer [1]		
κ	Permeability of the aquifer [m^2]		
K	Drained Bulk modulus of the aquifer [Pa]		
E_{aq}	Drained Young's modulus of the aquifer [Pa]		
ν_{aq}	Drained Poisson's ratio of the aquifer [1]		
ρ_{aq}	Drained density of the aquifer [kgm^{-3}]		
α	Biot-Willis-coefficient [1]		
E_c	Young's Modulus of the cap rock [Pa]		
ν_c	Poisson's ratio of the cap rock [1]		
ρ_c	Density of the cap rock [kgm^{-3}]		
E_h	Young's Modulus of the host rock [Pa]		
ν_h	Poisson's ratio of the host rock [1]		
ρ_h	Density of the host rock [kgm^{-3}]		
ΔP	Magma chamber pressurisation [Pa]		
β	Magma compressibility [Pa^{-1}]		
V	Magma chamber volume [m^3]		
L	Radial distance domain centre - aquifer [m]		
z_T	Depth of magma chamber top [m]		
r	Radius of the spherical magma chamber [m]		

Table 2. Input Parameters: reference values and ranges for parametric studies (where performed)

Parameter	Reference Value	Range
Aquifer depth z_{aq}	200 m	100 - 1000 m
Aquifer thickness d_{aq}	200 m	50 - 450 m
Chamber top depth z_T	3 km	1 - 5 km
Chamber radius (spherical) r	1 km	0.5 - 1.5 km
Horizontal half-radius b	1 km	0.25 - 3.5 km
Aquifer lateral onset L	0 km	0 - 8 km
Cap rock Young's Modulus E_c	70 MPa	
Host rock Young's Modulus E_h	30 GPa	
Aquifer Young's Modulus - pyroclastic E_{aq}	10 MPa	0.05 - 100 MPa
Aquifer Young's Modulus - lava flow E_{aq}	50 GPa	0.5 - 100 GPa
Cap rock Poisson's ratio ν_c	0.45	
Host rock Poisson's ratio ν_h	0.25	
Aquifer Poisson's ratio - pyroclastic ν_{aq}	0.275	0.15 - 0.4
Aquifer Poisson's ratio - lava flow ν_{aq}	0.225	0.1 - 0.35
Cap rock densityρ_c	1800 $\mathrm{kgm^{-3}}$	
Host rock densityρ_h	2600 $\mathrm{kgm^{-3}}$	
Aquifer density - pyroclastic ρ_{aq}	2000 $\mathrm{kgm^{-3}}$	
Aquifer density - lava flow ρ_{aq}	2800 $\mathrm{kgm^{-3}}$	
Aquifer permeability - pyroclastic κ	5×10^{-11} $\mathrm{m^2}$	10^{-14} - 10^{-7} $\mathrm{m^2}$
Aquifer permeability - lava flow κ	5×10^{-12} $\mathrm{m^2}$	10^{-14} - 10^{-9} $\mathrm{m^2}$
Aquifer porosity - pyroclastic ϕ	0.35	
Aquifer porosity - lava flow ϕ	0.1	
Biot Willis coeffient - pyroclastic α	0.7	0.35 - 1
Biot Willis coeffient - lava flow α	0.2	0.1 - 1
Water density ρ_f	1000 $\mathrm{kgm^{-3}}$	changed acc. to temperature changes, see Table 3
Water viscosity μ	10^{-3} Pas	changed acc. to temperature changes, see Table 3
Water compressibility χ_f	4×10^{-10} $\mathrm{Pa^{-1}}$	changed acc. to temperature changes, see Table 3
Pressurisation value ΔP	10 MPa	0.1-10 MPa

Table 3. Temperature dependent water properties for a pressure of 4.5MPa (calculated using Verma (2003))

Temperature (°C)	Density ρ_f (kgm^{-3})	Viscosity μ (Pas)	Compressibility χ_f (Pa^{-1})
10	1001.80	1.30×10^{-3}	4.73×10^{-10}
40	994.14	6.53×10^{-4}	4.37×10^{-10}
70	979.70	4.05×10^{-4}	4.46×10^{-10}
100	960.40	2.83×10^{-4}	4.83×10^{-10}
200	866.89	1.35×10^{-4}	8.64×10^{-10}
300	19.46	1.98×10^{-5}	2.60×10^{-7}
400	15.44	2.44×10^{-5}	2.38×10^{-7}
500	13.07	2.87×10^{-5}	2.31×10^{-7}

Table 4. Parameter and priority groups definition for the ranking resulting from sensitivity analysis

Parameter Group	$h* = \frac{\Delta h}{\Delta h_{ref}}$	$> 90\%$ of plots	$> 60\%$ of plots
A	$h* \geq 2.5$	Priority 1	Priority 2
	or $h* \leq -0.5$		
B	$1.9 < h* < 2.5$	-	Priority 3
	or $-0.5 < h* < 0.1$		
C	$0.1 \leq h* \leq 1.9$	Priority 4	-

Table 5. Nondimensional parameters used in parametric studies

Parameter	Pyroclastic aquifer	Reference	Lava flow aquifer	Reference
ν_c	0.15 - 0.4	0.45	0.15 - 0.4	0.45
ν_{aq}	0.275 - 0.4	0.275	0.1 - 0.35	0.225
ν_h	0.1 - 0.3	0.25	0.1 - 0.3	0.25
F	3.57×10^{-19} - 3.57×10^{-12}	1.79×10^{-15}	1.25×10^{-18} - 1.25×10^{-13}	6.25×10^{-16}
Q	1.59×10^{-3} - 4.89	4.89	4.91×10^{-2} - 0.943	9.38×10^{-2}
ER_l	0.001 - 200	1	1×10^{-6} - 0.02	2×10^{-4}
ER_h	50 - 2×10^{6}	3000	0.01 - 200	0.6
ER_c	0.01 - 2×10^{4}	7	1×10^{-5} - 2	1.4×10^{-3}
CD	10 - 25	15	5 - 25	15
CR	2.5 - 7.5	5	2.5 - 7.5	5
AD	1 - 5.5	1.5	1 - 5.5	1.5

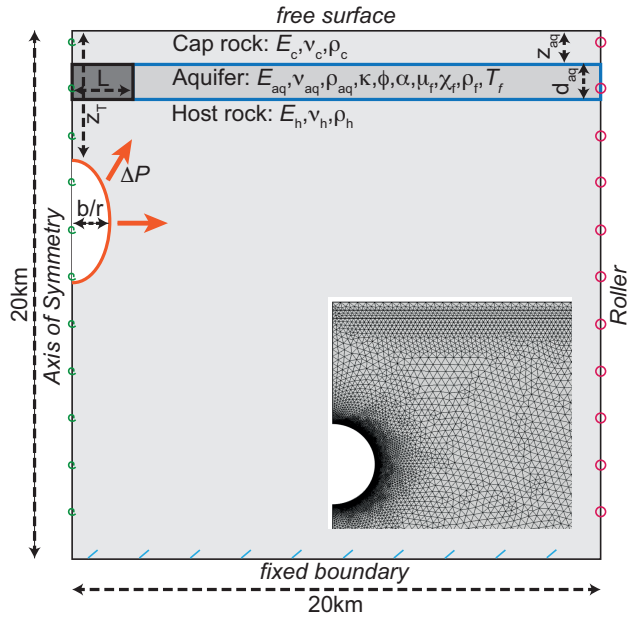

Figure 1. 2D axisymmetric model setup: a boundary load ΔP is applied on a cavity at depth, with the radius r for the spherical case or half-radius b for the ellipsoidal case, respectively. This changes the strain conditions in the surrounding linear elastic host rock (granitic crust), the poroelastic aquifer and the overlying linear elastic cap rock (clay). The water-saturated aquifer is modelled as either a vesicular lava flow or unconsolidated pyroclasts. An aquifer not covering the chamber but starting at some lateral distance L is realised by setting the darker grey region impermeable. The bottom boundary is fixed, the upper boundary is treated as a free surface, the lateral boundaries have a roller condition. There is no flow outside the aquifer, stress and displacement at the internal boundaries are continuous. An extract of the finite element mesh is shown only for illustration. The mesh density is finer around the cavity, at aquifer boundaries and the free surface.

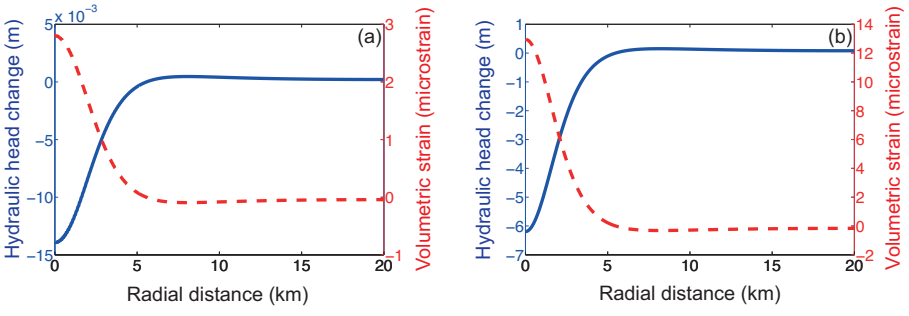

Figure 2. Results of the reference simulation, shown as the initial hydraulic head change and volumetric strain along profiles through the two aquifer types due to a magma chamber pressurisation of 10MPa: (a) pyroclastic aquifer, (b) lava flow aquifer. Both aquifers show a fall in hydraulic head mirroring the dilatational strain curves.

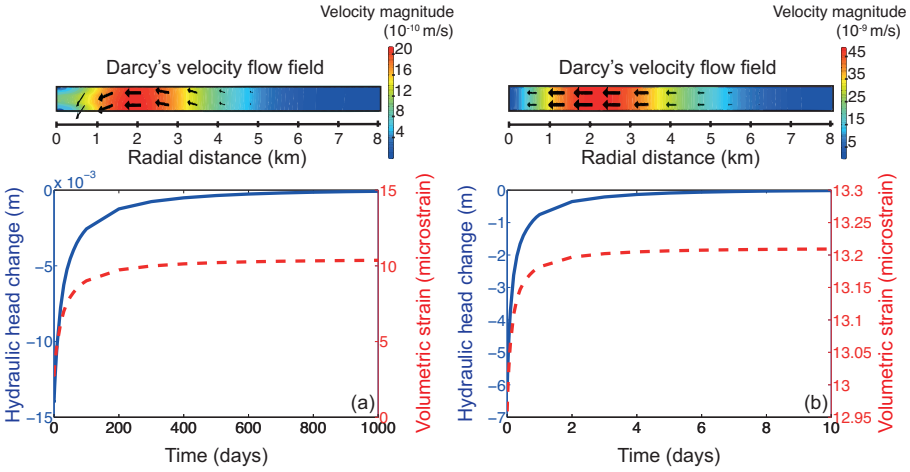

Figure 3. Upper graphs: porous flow pattern shown for the reference simulation at $t = 0.1$ days: (a) pyroclastic aquifer, (b) lava flow aquifer. Arrow length is proportional to flow velocity (note: different scales for a) and b)), colours show velocity magnitude. Lower graphs show hydraulic head and strain development with time in the centre of the aquifers, note the different time scale - flow processes are faster in the lava flow aquifer.

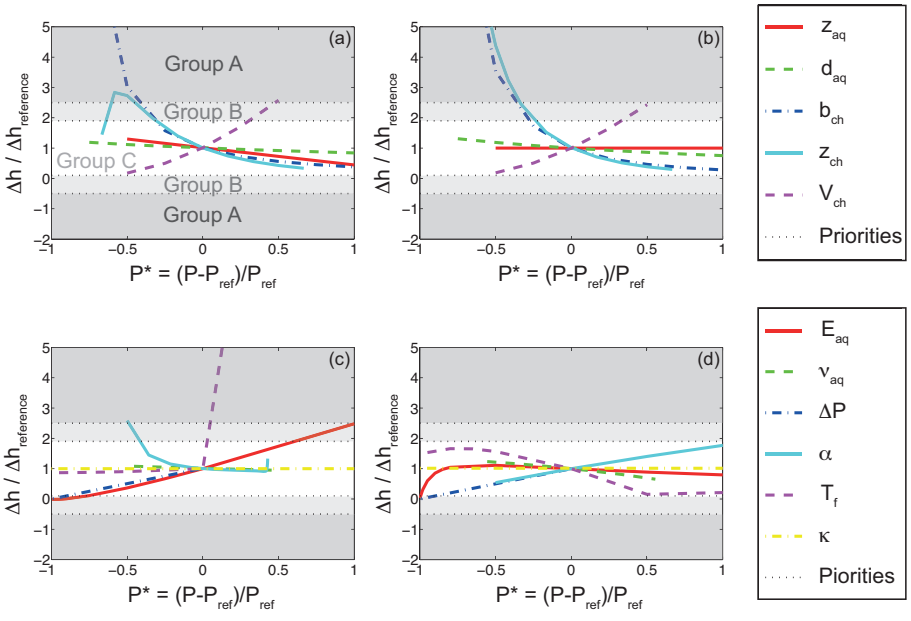

Figure 4. Exemplary plots used for the Sensitivity Analysis, showing the influence of changing a parameter (whilst keeping all others constant) on the central, initial hydraulic head change. (a), (c): pyroclastic aquifer, (b), (d): lava flow aquifer. Dashed lines/grey areas indicate the bounds that were used to rank parameters according to their importance. Pore fluid temperature, half radius of the ellipsoidal chamber and source depth are the most influential parameters shown here.

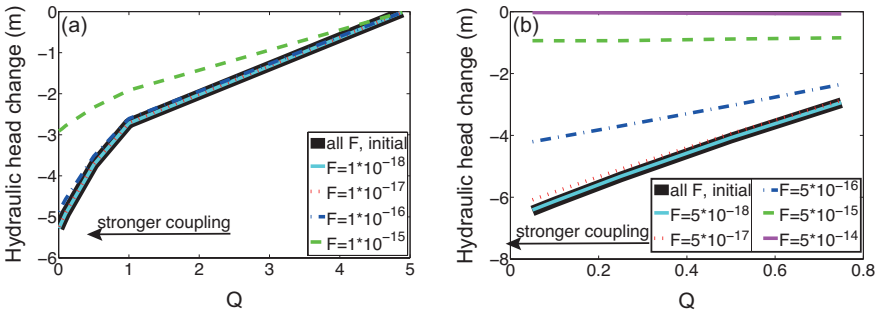

Figure 5. Influence of the non dimensional flow and coupling parameters Q and F, shown for the central hydraulic head change initially (thicker line) and after 1day (normal lines): (a) pyroclastic aquifer, (b) lava flow aquifer. F ($= \frac{\kappa}{\alpha d_{aq}^2}$) determines the porous flow velocity and hence how fast the initial hydraulic head gradient in the aquifer is equilibrated, while Q ($= \frac{\alpha}{S E_{aq}}$) determines the pressure response of the aquifer.

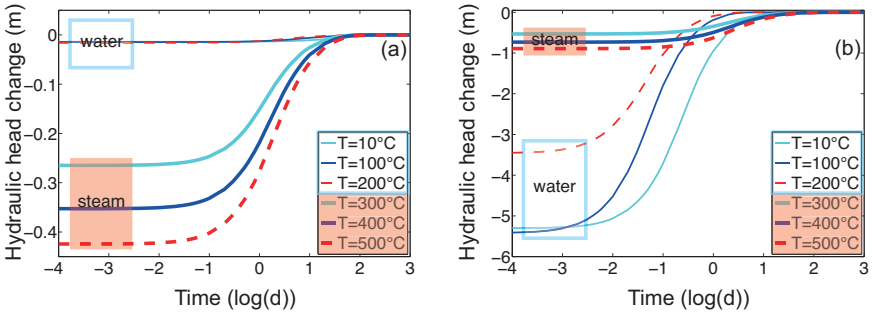

Figure 6. Central hydraulic head change and its evolution with time for different pore fluid temperatures: (a) pyroclastic aquifer, (b) lava flow aquifer.

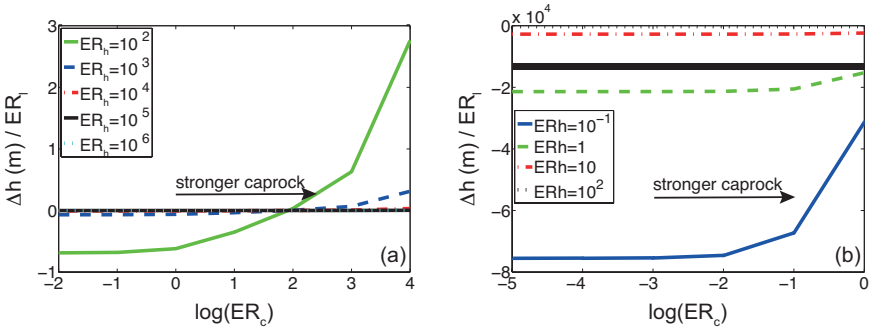

Figure 7. Influence of the elastic stratigraphy, shown using the nondimensional ER-Parameters: (a) pyroclastic aquifer, (b) lava flow aquifer. The initial, central hydraulic head change, scaled with the relative loading ER_l ($\mathrm{ER}_l = \frac{\Delta P}{E_{aq}}$), is plotted against relative stiffness of the cap rock ($\mathrm{ER}_c = \frac{E_c}{E_{aq}}$) for different relative stiffnesses of the host rock ($\mathrm{ER}_h = \frac{E_h}{E_{aq}}$).

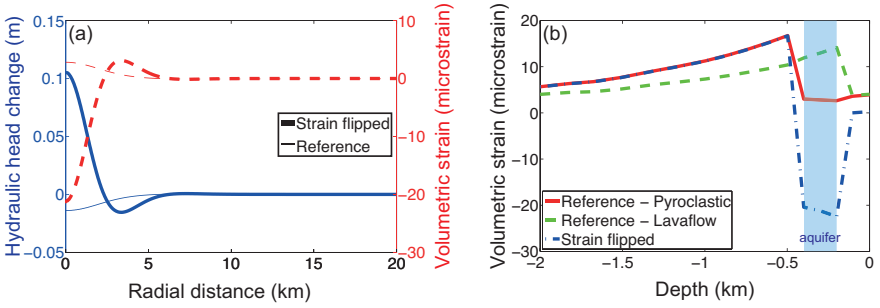

Figure 8. Effect of a sufficiently stiff caprock (ER_c=1e4) to flip the strain: (a) Horizontal profile through the aquifer showing the hydraulic head change and volumetric strain in the reference pyroclastic aquifer and the sign-flipped simulation (b) Vertical strain profiles through the centre of the domain from 2km depth to the surface, showing the jumps of volumetric strain when entering a different elastic layer for different elastic stratigraphies.

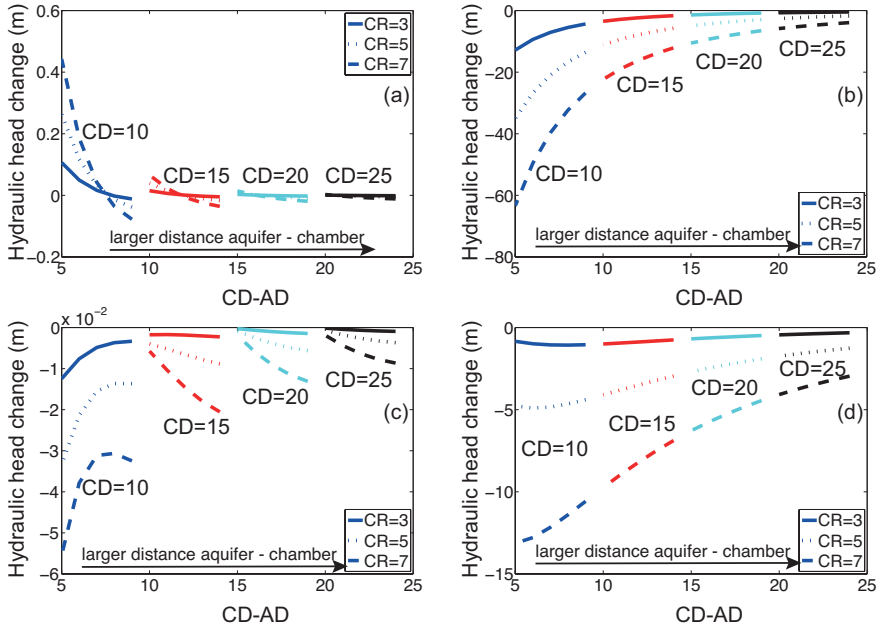

Figure 9. Influence of the geometry on the resulting initial hydraulic head change, central ((a) and (b)) and at 2km radial distance ((c) and (d)): (a) and (c) pyroclastic aquifer, (b) and (d) lava flow aquifer. Plotted are the nondimensional parameters AD= $\frac{z_{centeraq}}{d_{aq}}$, CR= $\frac{r}{d_{aq}}$ and CD= $\frac{z_T}{d_{aq}}$.

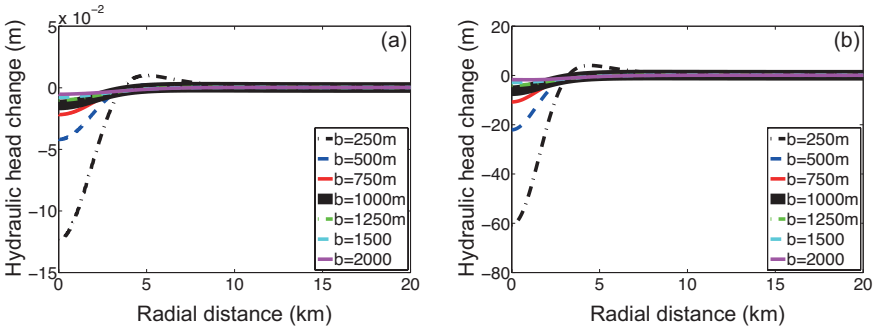

Figure 10. Influence of changing the aspect ratio of a spheroidal chamber (with constant z_T and V), shown as the initial hydraulic head change profile through the aquifer. Oblate shapes have b $<$ 1000m, prolate chambers correspond to b $>$ 1000m.

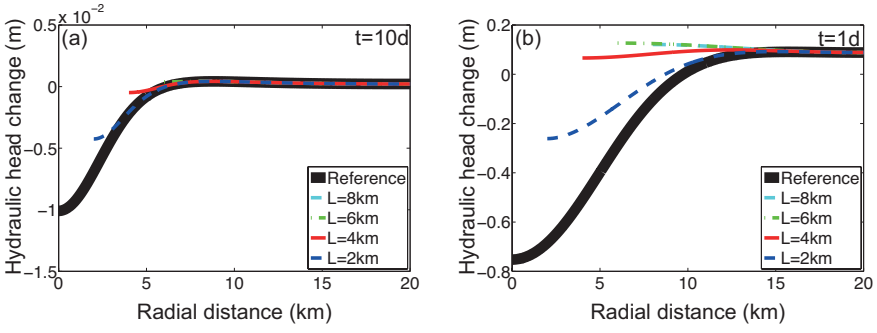

Figure 11. Influence of lateral distance L between chamber and aquifer, shown as the hydraulic head change profile through the aquifer after $t = 10\mathrm{d}$ (pyroclastic aquifer) and $t = 1\mathrm{d}$ (lava flow aquifer), respectively: (a) pyroclastic aquifer, (b) lava flow aquifer.

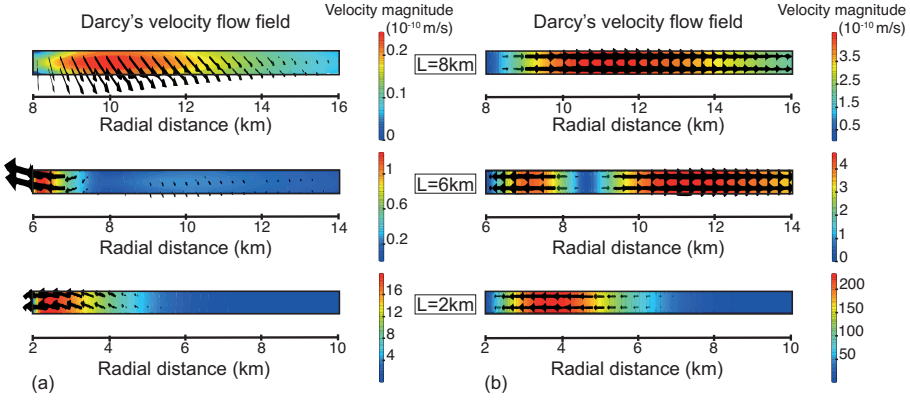

Figure 12. Influence of lateral distance L between chamber and aquifer on the flow pattern in the aquifers, here shown for t=0.1d for the first 8km of each aquifer: (a) pyroclastic aquifer, (b) lava flow aquifer. Arrow length is proportional to flow velocity (note: different scales for a) and b)), colours show velocity magnitudes.

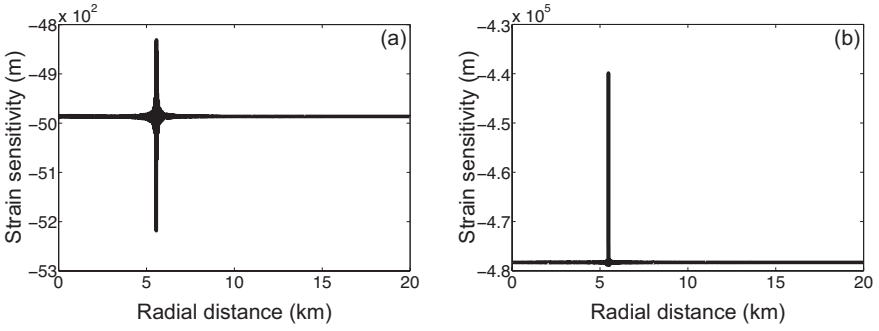

Figure 13. Strain sensitivity in the aquifers, determined by dividing simulated hydraulic head change by the volumetric strain, along a profile through the aquifers. Very small strains close to the transition zone from dilatational to compressional strain lead to numerical errors (reduced with increasing mesh density).

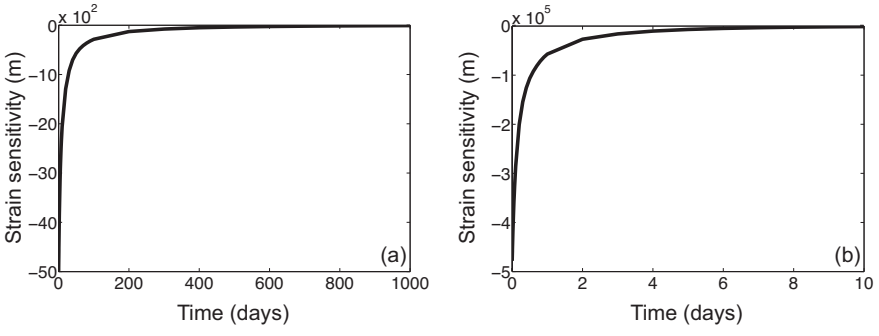

Figure 14. Strain sensitivity in the aquifers, determined in a point centrally above the chamber for different simulation times. The value strongly decreases with time, depending on flow processes in the aquifers.

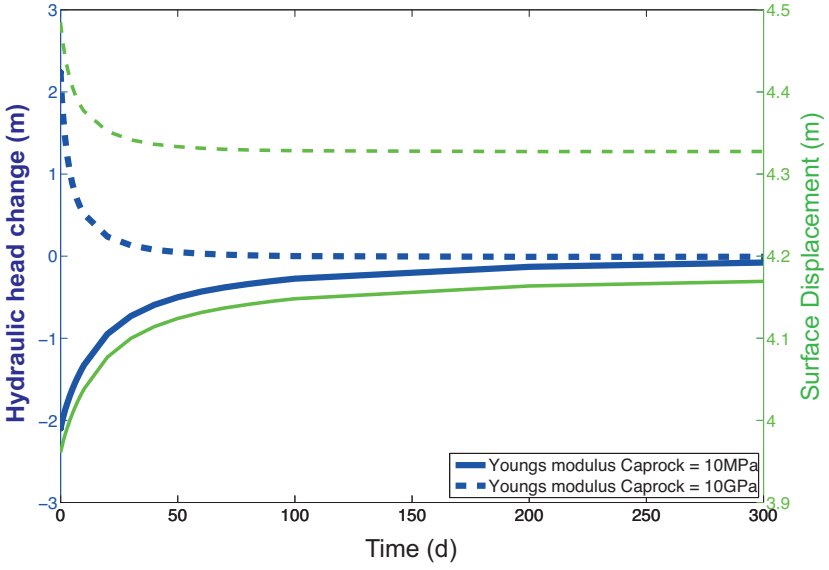

Figure 15. Central vertical surface deformation and hydraulic head change with time for the pyroclastic aquifer and different cap rocks, showing the effect of a sign-flipped strain in comparison to the reference case.

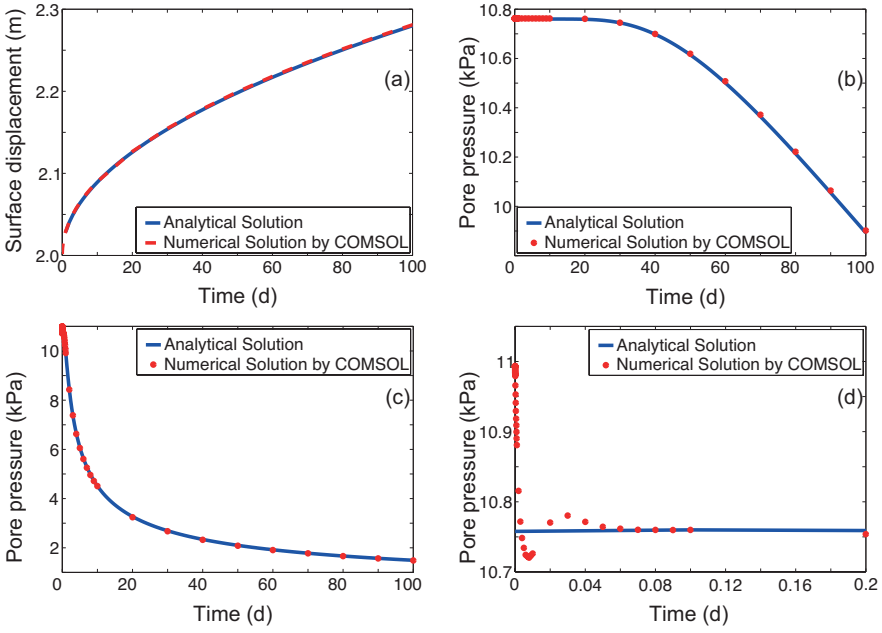

Figure A1. Results of benchmarking simulations: (a) total (downward) displacement of the surface (b) pore pressure at 1000m depth (c) pore pressure at 100m depth (d) pore pressure at 100m depth, zoom on the first 0.2s to illustrate numerical oscillation

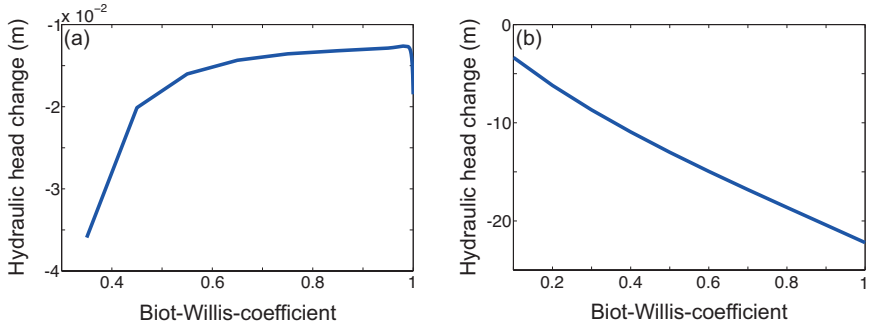

Figure B1. Dependance of central, initial hydraulic head change on the Biot-Willis-coefficient; (a) Pyroclastic aquifer (b) Lava flow aquifer

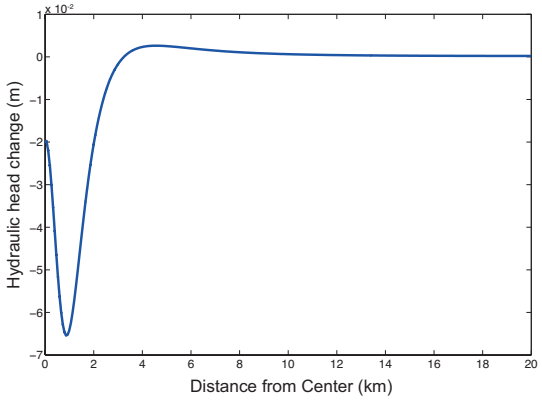

Figure C1. Hydraulic head change profile in the pyroclastic aquifer for CD=5, i.e. chamber depth of $1\mathrm{km}$